JTTEE5 19:1211–1217
DOI: 10.1007/s11666-010-9548-2
1059-9630/$19.00 © ASM International

Numerical Study of In-flight Particle Parameters in Low-Pressure Cold Spray Process

Xian-Jin Ning, Quan-Sheng Wang, Zhuang Ma, and Hyung-Jun Kim

(Submitted February 12, 2010; in revised form August 5, 2010)

A 2-D model of the low-pressure cold spray with a radial powder feeding was established using CFD software in this study. The flow field was simulated for both propellant gases of nitrogen and helium. To predict the in-flight particle velocity and temperature, discrete phase model was introduced to simulate the interaction of particle and the supersonic gas jet. The experimental velocity of copper powder with different sizes was used to validate the calculated one for low-pressure cold spray process. The results show that the computational model can provide a satisfactory prediction of the supersonic gas flow, which is consistent with the experimental Schlieren photos. It was found that similar velocity was obtained with the drag coefficient formula of Henderson and with that of Morsi and Alexander. As the shape factor was estimated, the reasonable prediction of velocity for non-spherical particle can be obtained, to compare with the experimental results.

Keywords cold gas dynamic spray, critical velocity, in-flight particle parameters, low-pressure cold spray, powder property

1. Introduction

The cold gas dynamic spray (CGDS, or cold spray) is relatively a new coating process that was developed in the last decade. In this process, the propellant gases of nitrogen or helium with pressure can be expanded using converging-diverging de Laval nozzle to generate a supersonic gas flow. The particle with a typical size of less than 50 μm can be fed into the gas flow, accelerated to a velocity of 300-1200 m/s, and then allowed to impact the substrate to deposit coating (Ref 1, 2). It is well known that in the cold spray process, there exists a critical velocity. Only the particles with an impact velocity higher than critical velocity can be deposited on the substrate to form coating (Ref 2, 3). In normal sense, the higher particle velocity and temperature can provide higher density, higher deposition efficiency, and the improvement of properties of coating (Ref 4). Therefore, the particle velocity and temperature become important factors during nozzle designing and modifications. Due to the limitation of experimental investigation, the computational method was introduced in previous studies to obtain the interaction between supersonic gas flow and particles (Ref 5-7). The in-flight particle velocity and effect of stand-off distance on

This article is an invited paper selected from presentations at the 4th Asian Thermal Spray Conference (ATSC 2009) and has been expanded from the original presentation. ATSC 2009 was held at Nanyang Hotel, Xi'an Jiaotong University, Xi'an, China, October 22-24, 2009, and was chaired by Chang-Jiu Li.

Xian-Jin Ning, Quan-Sheng Wang, and **Zhuang Ma**, School of Materials Science and Engineering, Beijing Institute of Technology, Beijing 100081, China; and **Hyung-Jun Kim**, Welding Research Center, RIST, Pohang 790-600, Korea. Contact e-mail: nxj@bit.edu.cn.

Nomenclature

u	velocity (m/s)
t	time (s)
F_D	drag force (N)
F_x	acceleration term (N)
μ	molecular viscosity (kg/m/s)
ρ	density (kg/m^3)
d	diameter (m)
C_D	drag coefficient
Re	Reynolds number
Ma	Mach number
γ	specific heat ratio
R	specific gas constant (J/kg/K)
T	temperature (K)
Φ	shape factor
h	convective heat transfer coefficient (W/m^2/K)
C_p	heat capacity (J/kg/K)
λ	thermal conductivity (W/m/K)
Nu	Nuselt number
Pr	Prandtl number of the continuous phase

Subscript

g	gas
p	particle
sph	spherical particle

particle impinging velocity were modeled using Henderson formula for high-pressure cold spray process (Ref 8). Based on the computational modeling, Li designed and optimized a CB nozzle by numerical method for high-pressure cold spray (Ref 9).

Besides the high-pressure cold spray, low-pressure cold spray was proven to be an effective method to deposit coatings under a much lower pressure which can significantly decrease the gas consumption and thus the cost (Ref 10, 11). However, few investigations were reported on the gas field and the particle acceleration for low-pressure cold spray process (Ref 4, 5). Moreover, the drag coefficient used in modeling for both high- and low-pressure cold sprays makes it difficult to confirm the modeling results of the particle parameters. Therefore, for the optimization of the spray nozzle and the better understanding of the spray process, a model of low-pressure cold spray process was established to obtain the particle parameters by CFD method in this study.

2. Numerical Methodology

The simulation of the gas flow and interaction of gas-particle were accomplished using commercial CFD software of Fluent (Fluent Inc., Lebanon, NH). The coupled implicit method provided in Fluent was chosen to simulate the gas flow in low-pressure cold spray. After the stable flow field was obtained, the particle velocity and temperature during the accelerating process in the gas flow were calculated using the discrete phase model (DPM).

2.1 The Computational Domain

Figure 1 shows the schematic of calculation domain. The cold spray process was performed using a converging-diverging barrel-type nozzle. The nozzle consists of a diverging part of 10 mm in length, a barrel part of 120 mm in length, and an exit size of 2.5 mm in radius. Nitrogen or helium with a pressure of 0.7 MPa and temperature of 573 K was used as a propellant gas. The powder is fed into the gas flow radially at the diverging part of 33.5 mm from nozzle throat by Venturi effect. To simplify the simulation model, the effect of feeding gas on the supersonic flow was neglected to establish a 2-D axisymmetric model. The outside domain is a cylinder of 30 mm in radius and 200 mm in length from the nozzle exit.

2.2 The Gas Flow

The propellant gas of cold spray process involves a compressible, viscous, turbulent, and normally supersonic gas flow. It is suggested that the viscosity changes with the temperature can affect the flow for the high-speed and compressible gas (Ref 12, 13). However, due to the relative low pressure and low temperature, the compressive nitrogen and helium used in this study were assumed to have a constant viscosity and obey the ideal gas law. Since the RNG k-ε model achieves the improved accuracy for rapidly strained flows than standard k-ε, the turbulence of the gas flow was simulated using the RNG k-ε model and standard wall functions (Ref 13).

2.3 Boundary Conditions

The inlet of nozzle was set as pressure inlet with a stagnation pressure (absolute) of 0.8 MPa and a stagnation temperature of 573 K. The exit of the outside domain was set as pressure outlet with a pressure and temperature of 0.1 MPa and 298 K, respectively. The nozzle wall was set as smooth, non-moving boundary, and with a heat flux of zero. The remaining part of the domain was set to be non-reflection boundary, as shown in Fig. 1.

2.4 The Interaction of Particle-Gas Flow

In DPM model, the particle is treated as discrete phase dispersed in the continuous phase, and the motion is calculated using Lagrangian formulation (Ref 13). Neglecting the gravity force, the balance force acting on the particle (in Cartesian coordinates) can be expressed as Eq 1:

$$\frac{du_p}{dt} = F_D + F_x \qquad \text{(Eq 1)}$$

The drag force per unit particle mass, F_D, can be expressed as Eq 2.

$$F_D = \frac{18\mu}{\rho_p d_p^2}\frac{C_D Re_p}{24}(u_g - u_p) \qquad \text{(Eq 2)}$$

where Re_p is the particle Reynolds number:

$$Re_p = \frac{\rho d_p |u_g - u_p|}{\mu} \qquad \text{(Eq 3)}$$

For spherical particle acceleration in the gas flow, the drag coefficient formula for the spherical particle was

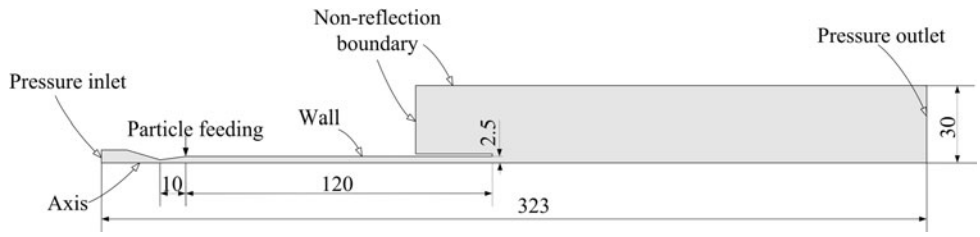

Fig. 1 The calculation domain of the low pressure cold spray model

taken from Morsi and Alexander (Ref 14) by default in Fluent:

$$C_D = a_1 + \frac{a_2}{Re} + \frac{a_3}{Re^2} \quad \text{(Eq 4)}$$

where a_1, a_2, and a_3 are constants (see Appendix A) that apply over several ranges of Re.

According to a previous study (Ref 12), the drag coefficient given by Henderson is more sensitive for the shock in the supersonic flow. Therefore, Henderson correlation was introduced to compare with the default Morsi and Alexander correlation in this study. In Henderson correlation (Ref 15), the drag coefficient involves both Reynolds and Mach number of the particles as presented in Eq 5-7:

For $Ma_p \leq 1$

$$C_D = 24\left(Re_p + (\gamma/2)^{1/2} Ma_p \left\{4.33 + \left(\frac{3.65 - 1.53\,T_p/T_g}{1 + 0.353\,T_p/T_g}\right) \times \exp\left[-0.247(2/\gamma)^{1/2}\frac{Re_p}{Ma_p}\right]\right\}\right)^{-1} + \exp\left(-\frac{0.5Ma_p}{Re_p^{1/2}}\right) \times \left[\frac{4.5 + 0.38\left(0.03Re_p + 0.48Re_p^{1/2}\right)}{1 + 0.03Re_p + 0.48Re_p^{1/2}} + 0.1Ma_p^2 + 0.2Ma_p^8\right] + 0.6(\gamma/2)^{1/2} Ma_p\left[1 - \exp\left(-\frac{Ma_p}{Re_p}\right)\right] \quad \text{(Eq 5)}$$

For $Ma_p \geq 1.75$

$$C_D = \frac{0.9 + \frac{0.34}{Ma_p^2} + 1.86\left(\frac{Ma_p}{Re_p}\right)^{1/2}\left[2 + \frac{4}{\gamma Ma_p^2} + 1.058\frac{1}{Ma_p}\left(\frac{2T_p}{\gamma T_g}\right) - \frac{4}{\gamma^2 Ma_p^4}\right]}{1 + 1.86\left(Ma_p/Re_p\right)^{1/2}} \quad \text{(Eq 6)}$$

For $1 < Ma_p < 1.75$

$$C_D = C_D(1.0, Re_p) + \frac{4}{3}(Ma_p - 1)\left[C_D(1.75, Re_p) - C_D(1.0, Re_p)\right] \quad \text{(Eq 7)}$$

where the particle Mach number was given as

$$Ma_p = \frac{|u_g - u_p|}{\sqrt{\gamma R T_g}} \quad \text{(Eq 8)}$$

For the non-spherical particle, the drag coefficient was taken from Haider and Levenspiel (Ref 16):

$$C_D = \frac{24}{Re_{sph}}(1 + b_1 Re_{sph}^{b_2}) + \frac{b_3 Re_{sph}}{b_4 + Re_{sph}} \quad \text{(Eq 9)}$$

where b_1, b_2, b_3, and b_4 are constants provided in Appendix B.

Under the assumption that the temperature of the particle is under the vaporization temperature and neglecting the temperature gradient inside the particle, the particle temperature during the accelerating process in the flow can be calculated as follows (Ref 13):

$$m_p C_{pp} \frac{dT_p}{dt} = hA_p(T_g - T_p) \quad \text{(Eq 10)}$$

where the convective heat transfer coefficient, h, is related to thermal conductivity of the gas and the diameter of particle by Nuselt number (Nu):

$$h = \frac{\lambda_g Nu}{d_p} \quad \text{(Eq 11)}$$

Nuselt number can be described as

$$Nu = 2.0 + 0.6Re_p^{1/2}\,\mathrm{Pr}^{1/3} \quad \text{(Eq 12)}$$

Prandtl number, Pr, is given by

$$Pr = (\mu C_{pg})/\lambda_g \quad \text{(Eq 13)}$$

2.5 The Particle Velocity Measurement

In this study, the previously measured in-flight particle velocity with Spraywatch® (Oseir Ltd., Tampere, Finland) at the position 10 mm away from the nozzle exit was directly introduced for the validation of the numerically predicted particle parameters. For velocity measurement, commercial copper powder of different sizes was used (Ref 17). Table 1 shows the particle size parameters measured by laser granular analysis. The details of the particle morphology and the experimental construction can be found elsewhere (Ref 17).

3. Results and Discussion

3.1 Gas Flow Field

Figure 2 shows the comparison between the calculated gas flow outside the nozzle and the experimental Schlieren photos. Since the Schlieren photo was obtained based on the different refractions of laser resulting from the differences in density of gas flow (Ref 18), the picture can be considered as density distribution of the gas field. The simulated density contour demonstrates that the simulated

Table 1 The particle sizes measured with laser granular analysis of the copper powder used in this study (μm)

	D5	D10	D50	D90	D95	Mean size
Size 1	9.3	11	20	32.5	37.5	21
Size 2	4	4.6	28	45.5	52	28
Size 3	7.5	13.5	38.7	58.4	62.5	37.9
Size 4	9	18.1	48.3	69.5	75	47
Size 5	4	9.36	64.8	95.1	105	62.4

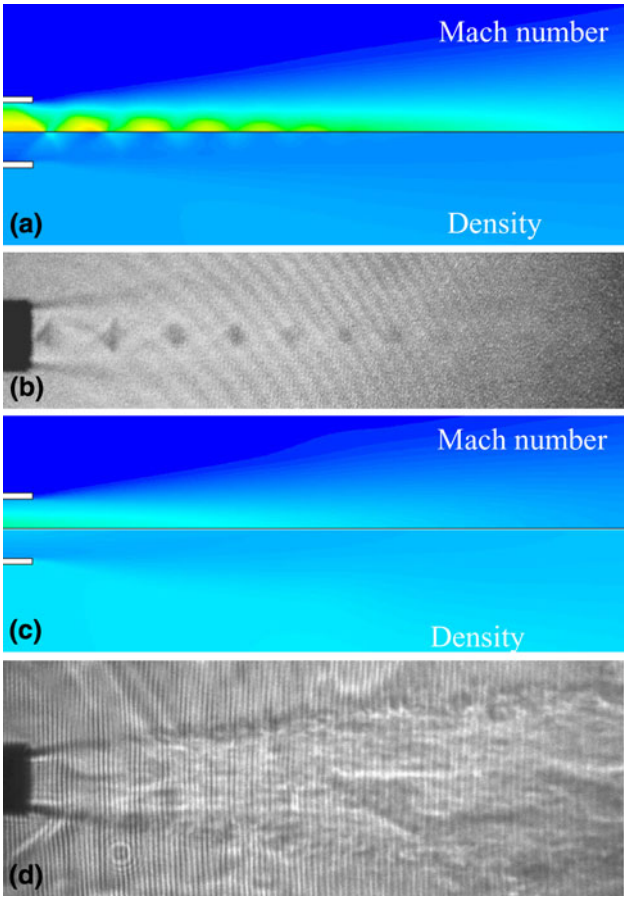

Fig. 2 The calculated contour of Mach number and density of the gas field outside the nozzle exit and Schlieren images: (a) calculated nitrogen flow, (b) Schlieren photo of nitrogen flow (Ref 9), (c) calculated helium flow, and (d) Schlieren photo of helium flow (Ref 9)

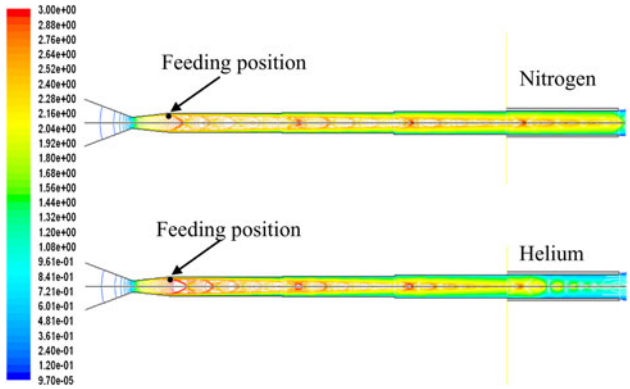

Fig. 3 The calculated Mach number contours of the flow inside the nozzle for nitrogen and helium propellant gas

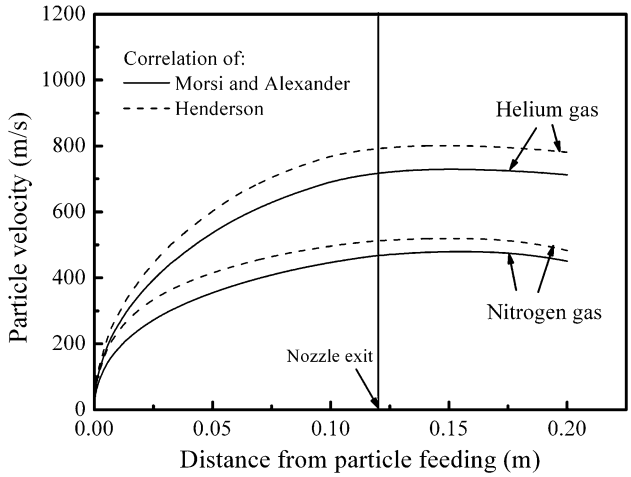

Fig. 4 The in-flight velocity of spherical copper particle with size of 10 μm in nitrogen and helium gas flows

nitrogen and helium gas flow is satisfactorily consistent with the experimental one. Moreover, it can be seen clearly that there exist a series of Mach diamonds. Among the Mach diamonds, high velocity and low density areas of the gas perform, which implies that the optimal standoff distance may depend significantly on the detailed gas flow.

Figure 3 shows the contour of Mach number inside the nozzle for nitrogen and helium gas. The sonic flow was obtained by the expansion, and the acceleration of the gas near the chocked throat for both nitrogen and helium. The oblique shock waves were formed at the connection area of diverging and barrel part due to the sharp change of the cross-sectional area inside nozzle.

As the low-pressure cold spray system performs, the powder is fed into the gas flow at the position just before the appearance of shock diamond. Since the static pressures of the feeding position (shown in Fig. 3) are 0.045 and 0.035 MPa for nitrogen and helium gases, respectively, the pressure difference between gas flow inside nozzle and the atmosphere resulted in the Venturi effect, which makes it possible for the powder feeding under the atmosphere in low-pressure cold spray process. When higher propellant gas pressure (e.g., more than 1 MPa) needs to be used, the additional pressure should be provided for the powder feeding gas.

It should be noted that near the nozzle exit, nitrogen performed an over-expanded flow which makes the oblique shock waves outside the nozzle exit due to the relative higher back pressure of environment, whereas for the helium gas, a thick boundary makes the flow velocity decrease dramatically to about 1 Mach in the center of the flow.

3.2 The In-flight Particle Parameters

The comparison of accelerating processes for a spherical copper particle of 10 μm with smooth surface using drag coefficient of Morsi-Alexander and Henderson is shown in Fig. 4.

Although it was suggested that the Henderson drag coefficient is sensitive to the shock waves in the gas flow and the bow shock near substrate (Ref 12), no obvious

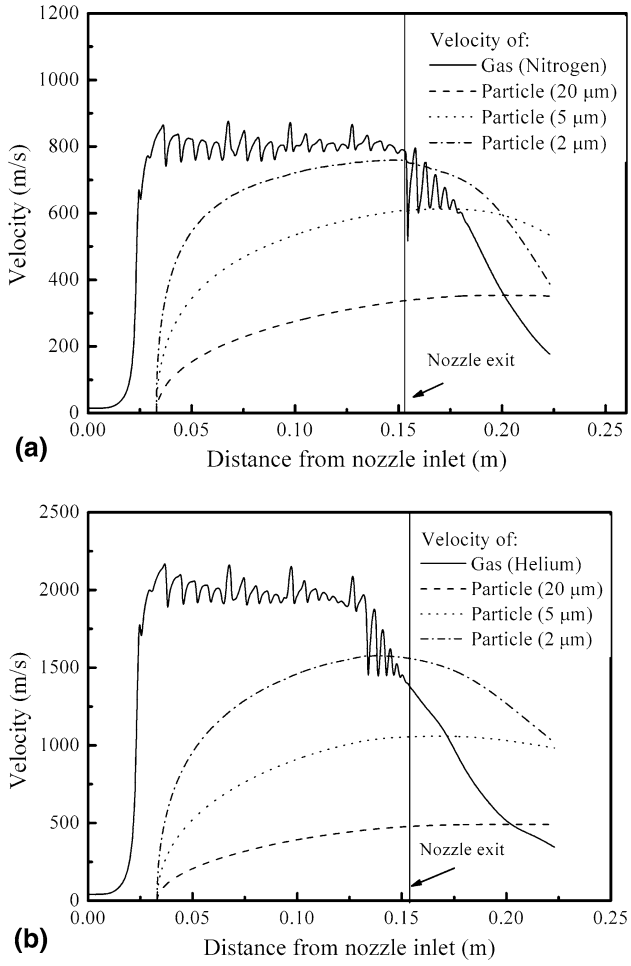

Fig. 5 The axial gas velocity and in-flight velocity of spherical copper particle of 2, 5, and 20 μm accelerated in nitrogen and helium gas flows: (a) nitrogen gas and (b) helium gas

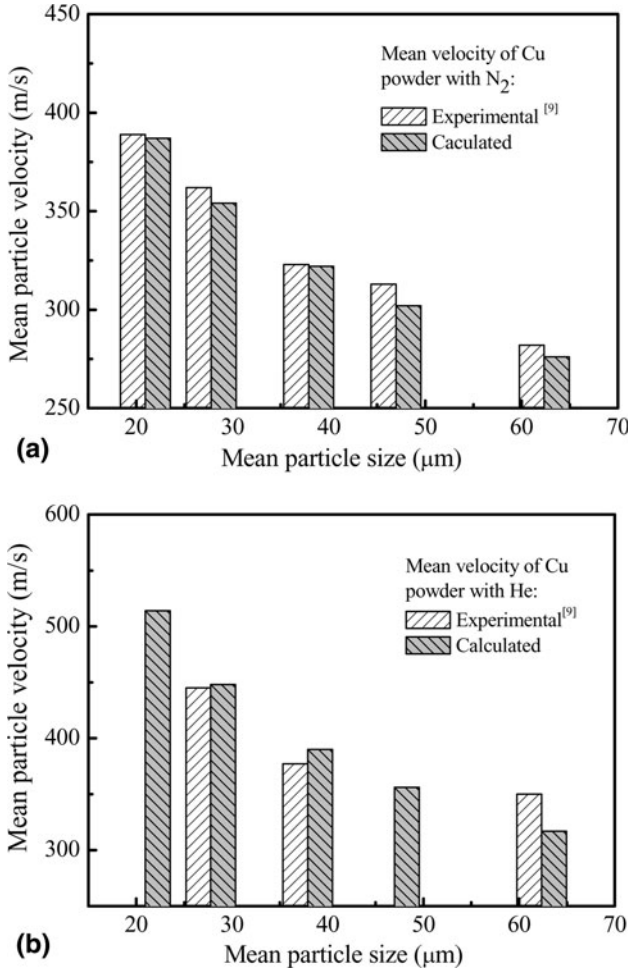

Fig. 6 The validation of the simulated in-flight velocity for non-spherical copper powder with different sizes: (a) in-flight particle velocity in nitrogen flow and (b) in-flight particle velocity in helium flow

difference of particle acceleration was observed in both nitrogen and helium gas flow. As the typical particle size of cold spray is 5-25 μm, it is suggested that the Morsi and Alexander correlation is prior for the prediction of particle in-flight velocity. Nevertheless, the velocity shown in Fig. 4 needs to be validated with further experimental data.

Figure 5 shows the velocity of spherical copper of different sizes accelerated by nitrogen and helium gas flow. As a comparison, the axial gas velocity was also presented. Although the Mach numbers for nitrogen and helium flows are close to each other inside the nozzle (shown in Fig. 3), the velocity of the latter is about 2.5 times that of the nitrogen flow due to the higher specific heat ratio (1.66), as well as the lower molecular weight of helium than that of nitrogen (1.4).

It is clear that the velocity of particle with a size less than 5 μm (e.g. 2 μm) was significantly influenced by the shock waves of gas flow away from nozzle exit. Nevertheless, the velocity can be kept unreduced to about 30 mm for 5 μm and over 40 mm for 20 μm due to the particle inertia. This implies that the normally used standoff distance of 10 mm can be extended to at least 30 mm for low-pressure cold spray. However, the previous research has pointed out that the longer distance may result in the decrease of the deposition efficiency and lower coating property due to the profile of the velocity in the cross plane outside the nozzle (Ref 19, 20).

Figure 6 shows the simulated in-flight velocity of 10 mm away from nozzle exit for non-spherical particle accelerated in nitrogen and helium gas flows using drag correlation of Haider and Levenspiel. For the near-spherical copper particles in this study, an estimated shape factor of 0.85 was obtained in Eq 9 by microscope and image analysis. Using the mean value of the particle size (VMD), a reliable in-flight velocity comparable with the experimental values can be obtained for a series of particle size in both nitrogen and helium gas flows.

One of the most important advantages of cold spray is that the particle experiences a much lower temperature

than in traditional thermal spray process. The same characteristic was observed in low-pressure cold spray in this study. The calculated temperature of copper particle with a size of 20 μm and an inlet temperature of 298 K can reach 284 K in nitrogen and, even 262 K in helium gas flows at the position 10 mm away from the nozzle exit. Although the accurate temperature of the particle is still not confirmed by experimental method, this low temperature feature makes low pressure cold spray a suitable method to deposit materials with low melting point such as Sn, Pb, and so on (Ref 21).

4. Summary and Conclusions

In this study, the 2-D computational model for low-pressure cold spray process was established based on the commercial CFD software Fluent to predict the in-flight particle parameters including velocity and temperature. The simulated gas field outside the nozzle exit is well consistent with the experimental Schlieren photos. Moreover, the performance of the nozzle used in this study is quite different for nitrogen and helium propellant gases. It was observed that the gas jet of helium presents separation near the nozzle exit, which can affect the uniformity of the particle velocity distribution along the cross section of the nozzle tunnel. Under the operating gas pressure of 0.7 MPa, a pressure difference of 0.035-0.045 MPa between internal gas jet and the environmental pressure, which provides the propellant force for powder feeding.

The drag coefficient is the most important factor in the DPM methodology after the steady continuous flow field was obtained. For non-spherical particles, the Haider and Levenspiel correlation can provide quite satisfactory results for particle in-flight velocity. For spherical-shape copper powder of 20 μm, the in-flight velocities 10 mm away from the nozzle exit present 484 and 343 m/s when accelerated by helium and nitrogen gases, respectively. However, when the size of the particle is decreased to 5 μm, a velocity of about 1058 m/s with helium gas, and 612 m/s with nitrogen gas can be obtained, each of which is much higher than the critical velocity of copper.Thus, if the small particle can be fed successfully into the low-pressure cold spray nozzle, then it can be expected that even under gas pressure of 0.7 MPa with low flow rate, effective deposition efficiency could be obtained. Although it has not been validated by experiment, the temperature of the particle obtained using the CFD model can provide an important reference of low-pressure cold spray in a few cases.

Acknowledgment

The authors gratefully acknowledge the support of Basic Research Program from Beijing Institute of Technology in the priority investigation of particle velocity and temperature of low-pressure cold spray.

Appendix A

The constants for Eq 4:

Re	a_1	a_2	a_3
<0.1	0	24	0
0.1-1	3.69	22.73	0.0903
1-10	1.222	29.1667	−3.8889
10-100	0.6167	46.5	116.67
100-1000	0.3644	98.33	−2778
1000-5000	0.357	148.62	−4.75E4
5000-10,000	0.46	−490.546	57.87E4
10,000-50,000	0.5191	−1662.5	5.4167E6

Appendix B

The constants for Eq 9:

$b_1 = \exp(2.3288 - 6.4581\Phi + 2.4486\Phi^2)$

$b_2 = 0.0964 + 0.5565\Phi$

$b_3 = \exp(4.905 - 13.8944\Phi + 18.4222\Phi^2 - 10.2599\Phi^3)$

$b_4 = \exp(1.4681 + 12.2584\Phi - 20.7322\Phi^2 + 15.8855\Phi^3)$

References

1. A.P. Alkimov, A.N. Papyrin, V.F. Kosarev, N.I. Nesterovich, and M.M. Shushpanov, ''Gas Dynamic Spraying Method for Applying a Coating'', U.S. Patent 5302414, 12 April 1994
2. V.F. Kosarev, S.V. Klinkov, A.P. Alkhimov, and A.N. Papyrin, On Some Aspect of Gas Dynamics of the Cold Spray Process, *J. Therm. Spray Technol.*, 2003, **12**(2), p 265-281
3. H. Assadi, F. Gätner, T. Stoltenhoff, and H. Kreye, Bonding Mechanism in Cold Gas Spraying, *Acta Mater.*, 2003, **51**(15), p 4379-4394
4. A.P. Alkhimov, V.F. Kosarev, and S.V. Klinkov, The Features of Cold Spray Nozzle Design, *J. Therm. Spray Technol.*, 2001, **10**(2), p 375-381
5. B. Samareh, O. Stier, V. Lüthen, and A. Dolatabadi, Assessment of CFD Modeling via Flow Visualization in Cold Spray Process, *J. Therm. Spray Technol.*, 2009, **18**(5-6), p 934-943
6. T.-C. Jen, L.-J. Li, W.-Z. Cui, Q.-H. Chen, and X.-M. Zhang, Numerical Investigations on Cold Gas Dynamic Spray Process with Nano- and Microsize Particles, *Int. J. Heat Mass Transf.*, 2005, **48**, p 4384-4396
7. T.-C. Jen, L.-P. Pan, L.-J. Li, Q.-H. Chen, and W.-Z. Cui, The Acceleration of Charged Nano-particles in Gas Stream of Supersonic de-Laval-Type Nozzle Coupled with Static Electric Field, *Appl. Therm. Engine*, 2006, **26**, p 613-621
8. J. Pattison, S. Celotto, A. Khan, and W. O'Neill, Standoff Distance and Bow Shock Phenomena in the Cold Spray Process, *Surf. Coat. Technol.*, 2008, **202**, p 1443-1454
9. W.-Y. Li, H.-L. Liao, G. Douchy, and C. Coddet, Optimal Design of a Cold Spray Nozzle by Numerical Analysis of Particle Velocity and Experimental Validation with 316L Stainless Steel Powder, *Mater. Des.*, 2007, **28**, p 2129-2137
10. A. Kashirin, O. Klyuev, T. Buzdygar, and A. Shkodkin, Dymet Technology Evolution and Application, *Thermal Spray 2007: Global Coating Solutions*, B.R. Marple, M.M. Hyland, Y.-C. Lau, C.-J. Li, R.S. Lima, and G. Montavon, Ed., May 14-16, 2007 (Beijing, China), ASM International, 2007, p 141-145
11. R. Tapphorn, H. Gabel, and J. Henness, Kinetic Metallization TM-Coating Development System, *Thermal Spray: Proceedings of the International Thermal Spray Conference*, B.R. Marple, M.M. Hyland, Y.-C. Lau, C.-J. Li, R.S. Lima, and G. Montavon, Eds., May 4-7, 2009 (Las Vegas, Nevada, USA), 2009, p 308-313
12. B. Samareh and A. Dolatabadi, A Three-Dimensional Analysis of the Cold Spray Process: Effect of Substrate Location and

Shape, *Thermal Spray 2007: Global Coating Solutions*, B.R. Marple, M.M. Hyland, Y.-C. Lau, C.-J. Li, R.S. Lima, and G. Montavon, Eds., May 14-16, 2007 (Beijing, China), ASM International, 2007, p 84-89
13. Fluent 6.2 User's Guide, Fluent Inc., Lebanon, NH
14. S.A. Morsi and A.J. Alexander, An Investigation of Particle Trajectories in Two-Phase Flow Systems, *J. Fluid Mech.*, 1972, **55**(2), p 193-208
15. C.B. Henderson, Drag Coefficient of Spheres in Continuum and Rarefied Flows, *AIAA J.*, 1976, **14**(6), p 707-708
16. A. Haider and O. Levenspiel, Drag Coefficient and Terminal Velocity of Spherical and Nonsperical Particles, *Powder Technol.*, 1989, **58**, p 63-70
17. X.-J. Ning, J.-H. Jang, and H.-J. Kim, The Effects of Powder Properties on In-flight Particle Velocity and Deposition Process During Low Pressure Cold Spray Process, *Appl. Surf. Sci.*, 2007, **253**, p 7449-7455
18. J. Anderson, *Fundamentals of Aerodynamics*, 3rd ed., McGraw-Hill Ryerson Ltd., New York, 2001, p 457-459
19. W.-Y. Li, C. Zhang, X.P. Guo, G. Zhang, H.L. Liao, C.-J. Li, and C. Coddet, Effect of Standoff Distance on Coating Deposition Characteristics in Cold Spraying, *Mater. Des.*, 2008, **29**, p 297-304
20. M. Karimi, A. Fartaj, G. Rankin, D. Vanderzwet, W. Birtch, and J. Villafuerte, Numerical Simulation of the Cold Gas Dynamic Spray Process, *J. Therm. Spray Technol.*, 2006, **15**(4), p 518-523
21. X.-J. Ning, J.-H. Jang, H.-J. Kim, C.-J. Li, and C. Lee, Cold Spraying of Al-Sn Binary Alloy: Coating Characteristics and Particle Bonding Features, *Surf. Coat. Technol.*, 2008, **202**, p 1681-1687